Journal of Building Engineering 94 (2024) 110012

Contents lists available at ScienceDirect

Journal of Building Engineering

journal homepage: www.elsevier.com/locate/jobe

Investigating the standard design and production procedure of heritage mortars for compatible and durable masonry restoration

Maphole Emelly Loke [a,*], Kumar Pallav [a], Giuseppe Cultrone [b], Chiara Di Filippo [c]

[a] Department of Civil Engineering & Geomatics, Faculty of Engineering and Built Environment, Cape Peninsula University of Technology, 1 Symphony Way, Bellville main campus, 7535, Cape Town, South Africa

[b] Departamento de Mineralogía y Petrología, Universidad de Granada, Fuentenueva, s/n, 18002, Granada, Spain

[c] Dipartimento di Scienze della Terra e dell'Ambiente, Università di Pavia, Ferrata 1, 27100 Pavia, Italy

ARTICLE INFO

Keywords:
Historical mortar
Design guideline
Mix design
Compatible restoration
Durability

ABSTRACT

Historic buildings ensure generational knowledge of past events, milestones, construction developments and evolution of materials, architectural designs, and practices throughout the centuries. It is indisputable that heritage buildings' survival against deterioration factors has proven the use of durable materials for their construction. However, they suffer inevitable decay due to ageing. Therefore, restoring the monuments to their original appearance and strength is always necessary for long-term survival. This paper discusses solutions for the design and development methods of new compatible restoration mortars for the architectural heritage, covering four significant aspects, namely: i) visual analysis of the heritage building in question, ii) experimental analysis of the original mortar samples for their physical, mineralogical and chemical properties, iii) characterization of the potential raw materials (available in the study area) that are close to the original, and iv) assessment of the new mortar durability. The mortars collected from the Castle of Good Hope, an important and ancient colonial edifice in the Western Cape Province (South Africa), were earth (samples SK7 to SK9) and hydraulic lime-based (SK1 to SK6), with 21–38 % porosity. The raw materials used on this monument include feldspar aggregates, possibly from the West Coast (Cape Town) and hydraulic lime for SK1, SK3 and SK5 mortars. For the restoration of the lime mortars (SK1, SK3 and, SK5), a hydrated lime-based mortar with a binder-to-aggregate ratio of 1:3, made of west coast sea sand and 5 % seashell additives, with a porosity of 24 %, has proved to be the most durable. The aesthetics for all the restoration mortars M1 to M9 is difficult to achieve considering the original material ageing factor, thus, the use of color-enhancing pigments is recommended.

1. Introduction

Buildings of historical significance bear witness to events that took place in past eras, exceptional architectural design and materials used to distinguish them from modern structures [1]. These features make the monuments stand out from the rest of the structures of recent times, thus attracting tourists to their respective countries. However, most of these structures are susceptible to various deterioration agents and must be repaired and maintained against potential environmental and anthropic attacks [2,3]. For this reason, the decayed parts of masonries, often mortars, which are considered sacrificial elements, are restored. Since the beginning of

* Corresponding author.
E-mail address: lokem@cput.ac.za (M.E. Loke).

https://doi.org/10.1016/j.jobe.2024.110012
Received 10 November 2023; Received in revised form 12 June 2024; Accepted 20 June 2024
Available online 21 June 2024

the 20th century, the original lime-based mortars have frequently been replaced with Portland cement [4]. This regrettable replacement is believed to have intensified the decay problem of historical masonries [5] and has left many of the heritage buildings enduring premature deterioration of such repairs [6]. The unsuitable materials are undesirable in terms of long-term economic feasibility, sustainability and authenticity of the architectural heritage of a culture [5]. Using inappropriate repair mortars demonstrates a gap between knowledge and practice regarding the design and production of heritage restoration materials [7,8].

The primary objective of this study is to provide a comprehensive guide to the identification of key mortar properties in the formulation and development of compatible mortars to be used in architectural heritage. The mortars developed in this paper can play a key role in preserving the historical and structural integrity of historical buildings, as in the case of the renowned Castle of Good Hope located in the Western Cape Province (South Africa). The Castle of Good Hope is one of South Africa's most profoundly significant heritage sites, encapsulating meaning for the nation itself and being of historical value for certain European regions like the Netherlands and the United Kingdom. The Castle's origins date back to 1666 when the Dutch East Indian Company (VOC) laid its foundational stone in the Cape [9]. The VOC, actively engaged in spice trade across Europe, Asia, and Africa, left an enduring mark on this structure. This colonial masterpiece, a testament to the VOC's architectural prowess, has stood the test of time and is arguably one of the best-preserved remnants of the VOC's global architectural endeavors. Much credit is due to the relentless efforts of the South

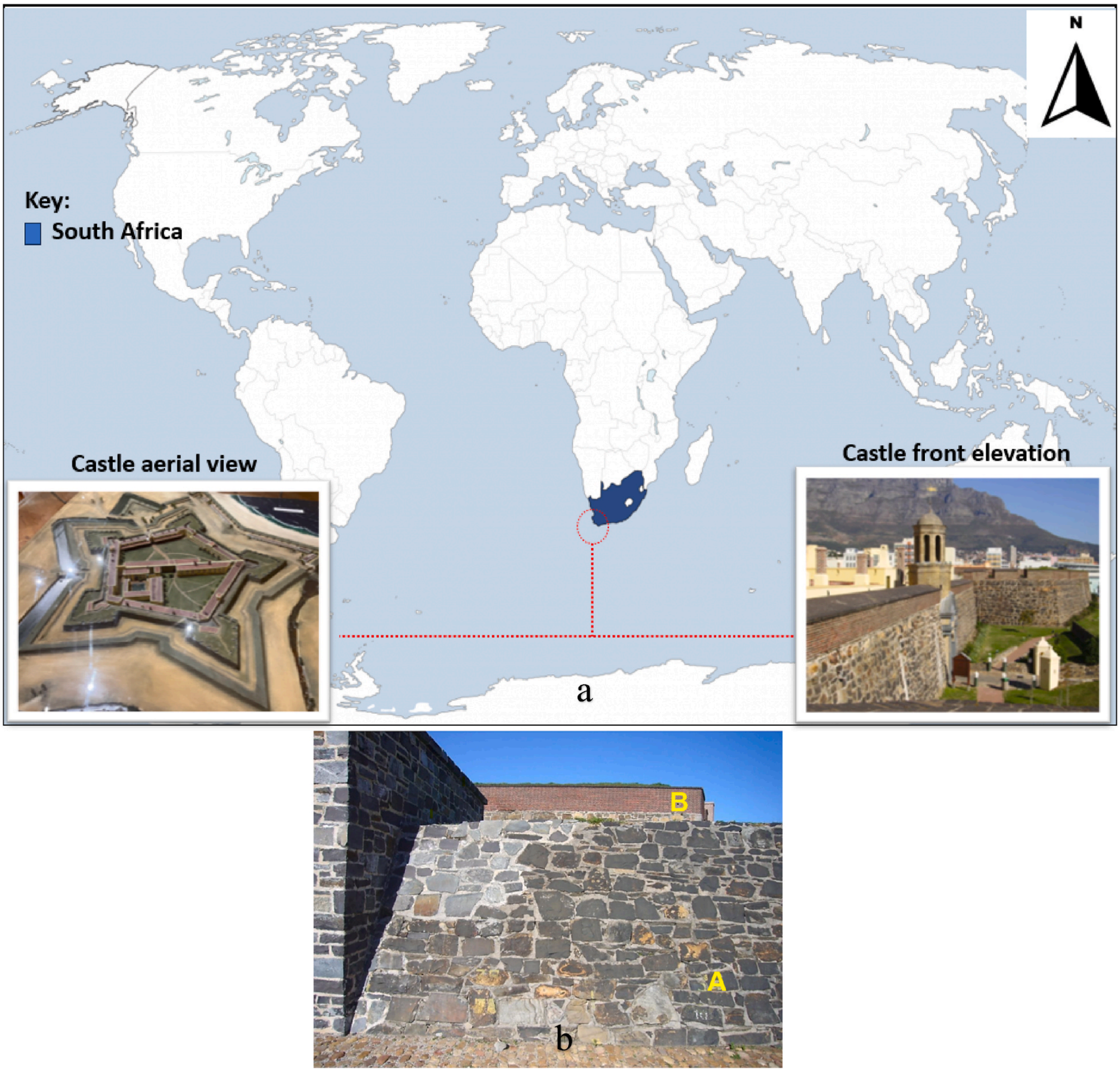

Fig. 1. a) Geographical map of South Africa and an aerial image of the Castle of Good Hope (on the left) and an elevation (on the right) showing the castle's entrance. b) The image below in the center illustrates A) The Dutch wall section constructed using blue slate and B) The British wall extension using reddish brickwork [10].

African Heritage Resources Agency to safeguard such valuable structures.

The distinctive architectural design of the castle's pentagon (Fig. 1a), characterized by its five principal bastions, offers a captivating aerial vista from Cape Town's heart, situated on Strand Street. Its construction involved the excavation of 3.5-m-deep foundations, followed by constructing 0.6-m-wide, 10-m-tall blue slate walls. In the 1830s, when the British took control of the Castle from the Dutch, they augmented the structure by raising the walls with reddish brickwork, as shown in Fig. 1b. Other changes made by the British included changing the previously flat slate roof to a pitched roof (source: https://www.castleofgoodhope.co.za/index.php).

The materials used to construct this monument were sourced from Signal Hill and Robben Island (Cape Town), with decorative clinker bricks imported from the Netherlands. Since 1922, the South African government has been responsible for overseeing the Castle's maintenance, which presently serves as the headquarters for the Western Cape Military and remains a prime attraction, drawing scores of tourists daily.

2. Design and production of heritage restoration mortars

Using suitable mortars in masonry restoration projects carries significant economic advantages. These advantages stem from the fact that when the proper mortar is applied, it often eliminates the need for costly repetitive restoration, as it effectively matches existing surface properties and ensures optimal performance. Consequently, carefully designing of mortars for restoration is an essential step in any conservation or restoration project involving historic or contemporary structures. Several heritage restoration projects have shown that the selection of restoration mortars for pre-existing masonry is challenging [11,12]. Up to now, the design of restoration mortars is, to some degree, still neglected by the scientific community [13,14]. This becomes a significant concern for structures of historical significance as the regrettable application of Portland cement, which is strongly discouraged on ancient buildings due to the different properties it portrays, still takes priority [15,16]. One possible reason for using inappropriate binders is a lack of understanding of the restoration of historic mortars. As shown in Fig. 2, the design of cement-based mortars (indicated in black) differs from that of lime-based mortars (in red). However, these differences are not extensively emphasized to prevent potential problems associated with material mismatches.

Even though it is agreed that the restoration of historic mortars is undoubtedly so important [18], warn of the complexity of this exercise. Researchers have made numerous proposals to address the challenge of abrupt failure in historic mortar restoration projects. However, there is still a lack of detail in the design and production of compatible mortars, with increasing attempts being made to produce industrial repair mortars from aerial or hydraulic lime with small amounts of cement. Such mortars have displayed high compressive and flexural strength, lower porosity and water absorption, and lower water vapor transmission than traditional lime mortars [19]. Thus, it is essential to establish a comprehensive, step-by-step design and production guideline to address past errors in restoring historic mortar. This may be a valuable resource for future restoration practitioners and industry manufacturers specializing in historic mortars. The question of which material is suitable for restoring or renewing the original fragments of the historic monuments remains unanswered [20]. Therefore, to ensure the long-term survival of heritage structures, it is necessary to integrate the knowledge gained from research and the construction materials industry to design and produce restoration mortars that are compatible with the materials present in historic buildings and are durable. Unfortunately, unlike the design of cement mortars, there is a lack of data on mortar requirements/criteria in terms of properties associated with different mortar categories.

2.1. Historic material testing and design standards

As gleaned from the literature, a fundamental aspect of ensuring durable repairs and prolonged structural integrity in historic buildings is the comprehensive characterization of the original materials, followed by their faithful replication in the restoration

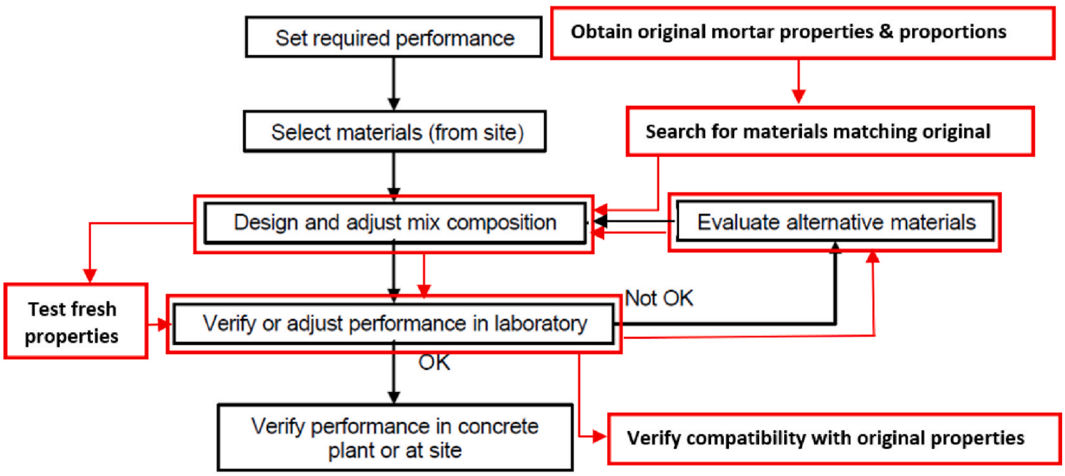

Fig. 2. Cement-based mortars design procedure versus historic lime mortar design procedure (highlighted in red) (modified from Efnarc [17]) showing the critical steps to be followed in the design process.

process [21]. This procedure is summarized in Fig. 3. The characterization process of original mortars is widely regarded as pivotal and indispensable in restoration, as it is perceived as the sole approach that guarantees harmony between original and repaired mortar surfaces. Simultaneously, it facilitates the early assessment of the durability of the developed mortars [22]. Nonetheless, incorrect procedure, analysis and interpretation during the study of original materials would yield a misleading choice of new ones, favoring premature failures in restoration works.

Generally, standards for designing and developing compatible and durable repair mortars are lacking in Africa. However, several international standards exist that contribute enormously to the design of heritage mortars. The modern construction industry relies on European (EN) and North American standards (ASTM) for test methods to manufacture and control the quality of ancient and modern mortars. The main difference between these standards and the RILEM recommendations is that the former refers to industrial mortars in which a hydraulic binder is used following the state of the mortar (fresh or hardened), while the latter focuses mainly on lime-based mortars and their final function (structural, grouting, pointing, flooring, rendering, plastering, etc.) making them more applicable to the heritage restoration concept.

The commonly used standard methods for concrete and mortars in South Africa are the South African National Standards (SANS) and the Cement and Concrete Institute Methods (C & CI). These two guidelines, like the ASTM, focus on the analysis of cement-based mortars and very little on lime-based mortars. C & CI provides even further detailed guidance on concrete mix design for specific target properties and highlights the details for different concrete applications, while elaborating on the standard properties of each category.

3. Experimental procedure

To propose compatible restoration mortars, a reverse engineering approach was used before making the new mortars. This process entailed a comprehensive and meticulous characterization of original samples carefully collected from various sections of Block B, the oldest segment dating back to 1666, within the Castle of Good Hope. Subsequently, based on these findings, new mortars were designed and formulated. Nine samples were collected from the monument and had distinct applications, including plasters, joints, and

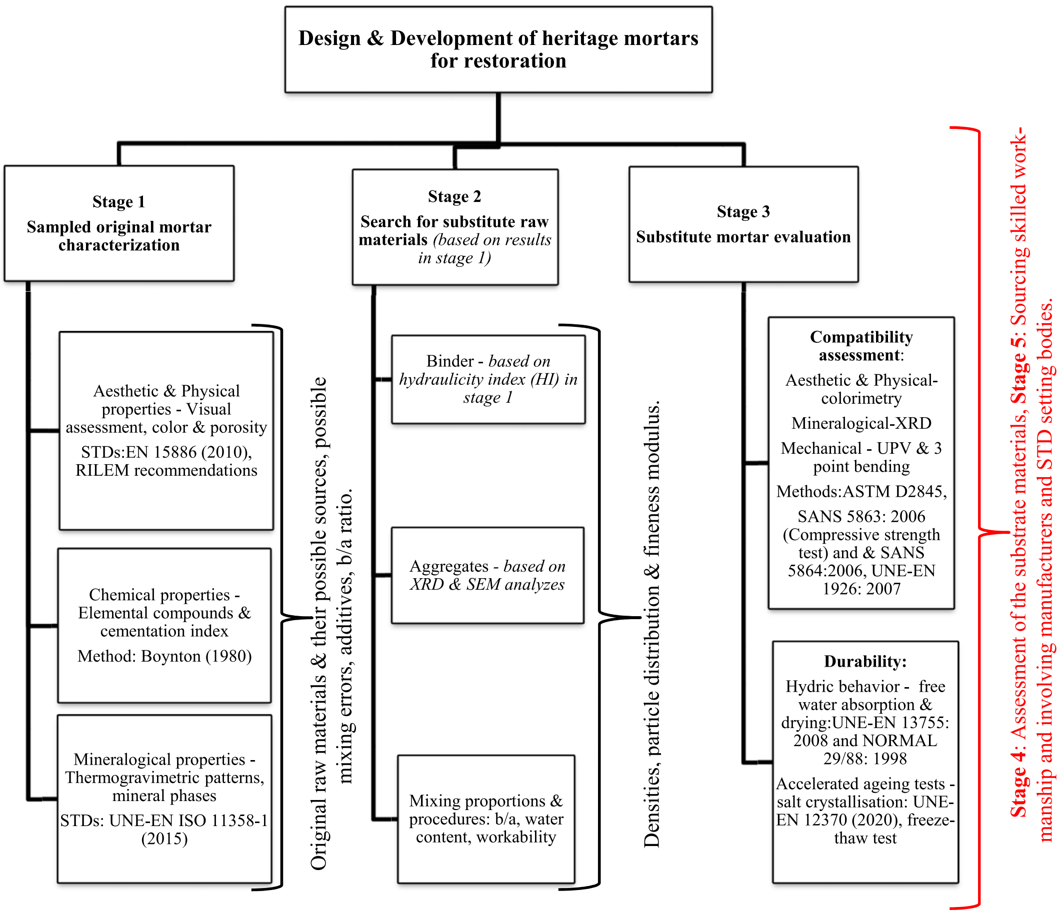

Fig. 3. The procedure for designing and developing compatible and durable heritage repair mortars with the first stage focusing on analysis of the originally sampled materials for their aesthetic, physical, mineralogy and chemical properties, stages two and three being a search procedure for repair raw materials and assessment of new mortars' compatibility and durability and finally stages four and five encompassing the assessment of the mortar substrate materials and ensuring the use of skilled mason for restoration work.

flooring. Different analytical techniques were used to study the properties of the original and newly manufactured mortars.

Relevant historical data on the construction and use of materials, visual and photographic survey, and restoration history were collected and critically analyzed. Sampling was carried out carefully with a chisel and small hammer according to Ref. [23] and using a sample information table recommended by Ref. [11].

3.1. X-ray fluorescence (XRF)

The major elements of mortar samples were determined by X-ray fluorescence (XRF) using a PANalytical Zetium compact spectrometer. Finely crushed samples of approximately 5 g were required for the analysis. XRF allowed us to calculate the cementation (CI) and hydraulicity indices (HI) through Equations (1) and (2), derived by Boynton (1980):

$$CI = \frac{(2.8 \text{ x } \%SiO_2 + 1.1 \text{ x } \%Al_2O_3 + 0.7 \text{ x } \%Fe_2O_3)}{(\%CaO + 1.4 \text{ x } \%MgO)} \quad (1)$$

$$HI = \frac{SiO_2 + Al_2O_3}{CaO} \quad (2)$$

3.2. Powder X-ray diffraction (PXRD)

The mineralogy of binder and aggregates was studied using a Panalytical X'Pert PRO diffractometer. The following operating conditions were followed: 45 kV voltage, 40 mA current intensity, 3–70° 2θ explored area and 0.01 2θ/s goniometer speed. Roughly 2 g fine powder samples were analyzed, and the diffractograms were processed with X'Pert HighScore Plus 3.0 software to identify the mineralogical phases present in original samples and new mortars throughout different carbonation stages.

3.3. Thermogravimetry and differential scanning calorimetry (TG-DSC)

The thermal decomposition of mortars was assessed by thermogravimetry and differential scanning calorimetry (TG-DSC) using a Mettler-Toledo TGA/DSC1. 50 mg per sample was used to measure their' weight loss during heating up to 950 °C.

3.4. Environmental scanning electron microscopy (ESEM)

An environmental scanning electron microscope (ESEM) QEMSCAN 650F was used to provide high-resolution images of mortars' texture and determine the crystal compound through energy dispersive X-ray spectroscopy (EDS) Bruker Quantax Esprit. Carbon-coated fragments of ~2 mm^3 in size were analyzed after being cleared of dust/dirt. This ESEM used an accelerating voltage of 10 kV with different magnification ranges.

3.5. Mercury intrusion porosimeter (MIP)

A Micromeritics AutoPore V 9600 porosimeter was used to determine the pore size distribution, open porosity (%), pore surface area (m^2/g), and bulk and skeletal densities (g/cm^3) of two original mortars, SK1 and SK5, whose dimensions allowed this type of analysis. About 1 g mortar fragments were oven-dried for 24 h and then analyzed.

3.6. Colorimetry

The color of mortar samples was quantified with a portable Konica Minolta CM-700d spectrophotometer using a color temperature of 6504 K in accordance with EN 16085 (2012) [23] standard. Lightness (L*), chromatic parameters (a* and b*), chroma (C*) and hue angle (h°) were determined. For each mortar sample, 3 measurements were made. The color difference (ΔE) between the original and new mortars was determined according to the following equation:

$$\Delta E = \sqrt{(L_1^* - L_2^*)^2 + (a_1^* - a^*{}_2)^2 + (b_1^* - b_2^*)^2} \quad (3)$$

Where:

L_1^*, a_1^*, b_1^* represent the lightness and chromatic values of original mortars,

$L_2^*, a^*{}_2, b_2^*$ represent the lightness and chromatic values of new repair mortars.

ΔE below 1 indicates no color difference, while the ΔE at 3.5 and above denotes a color difference perceptible to the human eye between the two measured surfaces [24].

4. New mortar materials and characterization

For compatibility, durability and cost effectiveness purposes, a type A2P (South African Bureau of Standards 523) building and plastering dolomitic (derived from deposits of 80 % CaO + MgO, 45 % CaO calcined and 5 % CO_2) pressure hydrated lime (air-hardened) produced by a nearby lime company (Afrimat Cape Lime quarry located at Langvlei, in the Western Cape Province) was used. This type of hydrated lime (alternative to hydraulic lime) was the closest to the original replacement material, as hydraulic lime could not be sourced in the study area. In terms of aggregates and additives, sand sourced from the Atlantic Ocean along the West Coast, similar to the original aggregates of sedimentary origin, was used with seashells as additives. The decision to use this type of sand was based on the need to minimize restoration costs (purchasing aggregates) on raw materials especially for the large-scale restoration. Considering that the Castle is located in a coastal area where sea sand could be a readily available raw material, the cost effectiveness of using sea sand could be beneficial.

The practice of using sea sand as aggregates in mortars was present since Roman times and is supported by Refs. [25–27]. However, as noted by Refs. [11,28], cations such as sodium and potassium and excess chlorides are a major concern when using marine aggregates. These authors suggest that in the production of mortar, it is necessary to use aggregates that are free from impurities, especially salt, in order to avoid salt crystallization in the masonry and corrosion of reinforcement in concrete structure [25,27]. In order to mitigate the effects of these elements on the properties of mortar, the sand collected from the Sea Point beachfront (on the west coast of the Atlantic Ocean) with a fineness of 3.84 (S gradation curves for mean of 3 tests per sand, Fig. 4) was soaked in potable water (free from impurities) for 48 h and washed thoroughly before mixing. Different amounts of seashells of different particle sizes were added to match the new mortars to the origi-nal composition. This was done because the naked eye easily distinguished shell fragments in the original mortars with the visual assessment. The control sample (M1) was produced from hydrated lime and coarse-grained commercial Philippi dune sand with a 1.64 fineness modulus as determined through an experimental sieve analysis (P gradation curves, Fig. 4). Shivakumar et al. [29] suggest that the grain size between 0 and 4 mm provides the highest compressive strength, while bigger grains reduce the mortar strength. This study's particle size distribution test follows the SANS 3001-AG1 (2014) [30] standard. Finally, a commercial calcium carbonate with a fineness modulus of 1.48 (Fig. 5) was used on mix 3 (M3) to replace seashells. Most of the powder $CaCO_3$ (80 %) used had particle sizes below 0.6 mm.

The mixing ratios for lime-to-aggregate of 1:3 by weight as suggested by Refs. [29,31] and 1:1 by weight as suggested by Ref. [5] were selected for optimization. A total of six mixes were prepared as follows:

Mix 1 (M1) - 1:3 hydrated lime, Philippi dune commercial sand (control mix).
Mix 3 (M3) - 1:3 hydrated lime, Philippi dune commercial sand, 10 % commercial calcium carbonate (control mix).
Mix 4 (M4) - 1:3 hydrated lime, Sea Point beachfront sand, 5 % finely (0.5–5 mm) crushed seashells.
Mix 6 (M6) - 1:3 hydrated lime, Sea Point beachfront sand, 5 % medium (5–15 mm) crushed seashells.
Mix 7 (M7) - 1:3 hydrated lime, Sea Point beachfront sand, 5 % finely (0.5–5 mm) crushed seashells, 3 % gypsum.
Mix 9 (M9) - 1:1 hydrated lime, Sea Point beachfront sand, 5 % medium (5–15 mm) crushed seashells.

The dry raw materials were first mixed, and then, on average, water to binder ratio of 0.73 for 1:3 mixes and 0.95 for M9 mortar were used. An automatic mortar mixer was used to knead the mortar and achieve the optimum consistency, allowing the mortars to dry at the recommended speed of 5–7 days, as specified in EN 998–1 (2003) standard before casting the 40 × 40 × 40 mm mortar cubes. The cubes were made by filling the freshly mixed mortar into molds at half capacity and gently compacting with a steel rod fifteen times, adding the mortar to full capacity and repeating the compaction. The mortar samples were dried under controlled temperatures (20 ± 5 °C) and humidity (60 ± 5 %) following the procedure by Ref. [32]. After demolding, the samples were left curing for 28, 60 and

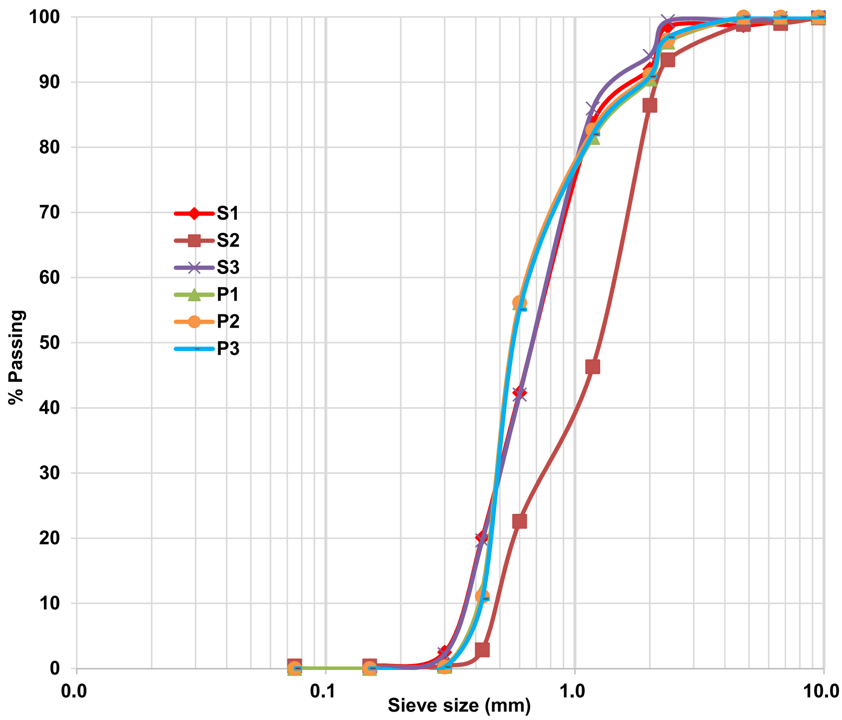

Fig. 4. Commercial Philippi dune and Sea Point beachfront sands distribution using [30]method. Three measurements per sand type were performed. S1–S3 represent the Sea Point sand gradation curves while P1–P3 represent the Philippi sand gradation curves.

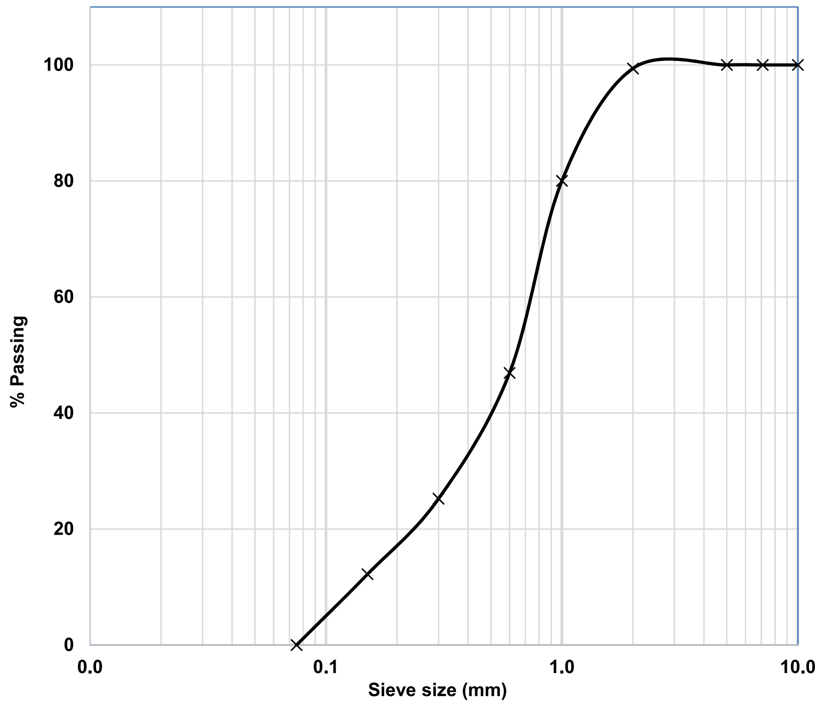

Fig. 5. Particle size distribution for commercially sourced calcium carbonate ($CaCO_3$) powder replacing seashells in new mortars.

90 days before any experiments were conducted on three samples per mortar type. A summary of the new repair mortars elaborated in this research and their match with the original samples is shown in Table 1.

4.1. Compatibility

To evaluate the compatibility of new repair mortars with the original, colorimetry and powder X-ray diffraction (PXRD) were used, following the same procedures as for the original mortar samples. Moreover, PXRD analysis was performed on the same sample's inner and outer layers to check the degree of carbonation due to the different exposure to carbon dioxide.

4.2. Hydric behavior

Water plays a significant role in construction materials' deterioration; thus, evaluating the absorption and drying kinetics of mortars is fundamental to analyze microstructural attributes (i.e. water flow in the pore network) and understand their durability [33, 34] Three cubes (40 × 40 × 40 mm) per new mortar mix after 60 ± 5 days curing time were tested to determine free and forced water absorption (A_b and $A_{f,}$ respectively) and drying following RILEM Recommendations (1980) [35], UNE-EN 13755 (2008) and NORMAL 29/88 (1998) standards. The pore interconnection degree (Ax), drying index ($D_{i)}$, saturation coefficient (S), open porosity (P_o) and the apparent (ρa) and real densities (ρr) were calculated.

Table 1
List of new repair mortars produced based on general features of original mortars deduced after visual observation.

Original Sample ID	Mortar Category	Original Mortar type	New repair mortars	New repair mortars, lime-to-aggregate ratio (by weight)
SK1	Plaster	Lime	M7	1:3
SK2	Plaster	Lime	M7	1:3
SK3	Plaster	Lime	M7	1:3
SK4	Floor	Lime	M4	1:3
SK5	Bedding/joints	Lime	M6	1:3
SK6	Bedding/joints	Lime	M9	1:1
SK7	Bedding/joints	Earth	–	
SK8	Bedding/joints	Earth	–	
SK9	Bedding/joints	Earth	–	
			–	
			–	
			–	

Table 2
X-ray fluorescence results of major oxides (in wt.%) except Zr (in ppm) used for computing the hydraulicity (HI) and cementation (CI) indices. LOI stands for loss on ignition and - for not detected.

ID	SiO_2 (%)	Al_2O_3 (%)	Fe_2O_3 (%)	MnO (%)	MgO (%)	CaO (%)	Na_2O (%)	K_2O (%)	P_2O_5 (%)	Zr (ppm)	LOI (%)	TOTAL (%)	HI	CI	Binder description, according to Brosnan (2014)
SK-1	2.94	0.47	0.19	–	0.27	53.32	0.63	0.17	0.14	65.4	41.58	99.76	0.06	0.17	Sub-hydraulic lime
SK-2	25.30	5.89	2.09	0.05	6.08	27.60	2.21	1.58	0.26	280.7	27.9	99.27	1.13	2.18	Unclassified
SK-3	2.61	0.42	0.18	–	0.18	53.03	0.69	0.17	0.13	59.4	42.31	99.77	0.06	0.15	Sub-hydraulic lime
SK-5	6.85	1.44	0.58	0.01	0.20	48.87	0.55	0.53	0.10	73.6	40.59	99.82	0.17	0.43	Slightly hydraulic lime
SK-7	47.27	12.89	3.96	0.02	0.68	11.93	2.85	1.66	0.17	499.0	16.98	99.09	5.04	11.59	Unclassified
SK-8	60.47	14.67	7.70	0.04	0.84	1.51	1.69	1.75	0.11	878.4	10.2	99.76	49.76	71.05	Unclassified
SK-9	60.12	17.47	5.60	0.02	0.72	3.30	0.40	2.05	0.14	357.8	8.84	99.55	23.51	44.45	Unclassified

4.3. Compactness and mechanical performance

The compactness and strength of mortars are of huge importance since they are interlinked with the mechanical performance of the entire building [36]. The new mortars' compactness was determined by a non-destructive technique, ultrasound. An ultrasonic pulse velocity tester (Controls 58-E4800) with 54 Hz frequency transducers was used on 3 samples per mortar type to evaluate their compactness. The direct transmission method [37] was used following the ASTM D2845 (2005) standard. Equation (4) was used to calculate the total anisotropy (ΔM) [38]:

$$\Delta M = \frac{V_{max} - V_{min}}{V_{max}} \times 100 \tag{4}$$

Where:

V_{max} is the maximum velocity of the three tests measured irrespective of the measurement direction,
V_{min} is the minimum velocity of the three tests measured, irrespective of the measurement direction.

The compressive strength of the new mortars was analyzed by means of uniaxial compression tests following the methodology by Cristofaro et al. [39]. The cubes of 40 × 40 × 40 mm with three curing periods of 28, 60 and 90 days were analyzed. A digital compression universal testing (Foote test press auto) machine at 50 kN/min loading speed was used on five samples per mortar mix. The test followed SANS Method 5863 (2006) with modifications aligning to UNE-EN 1926 (2007) standard.

4.4. Durability

To assess the damage emerging from filling the mortar pores and fissures with soluble salts, a set of 3 by 40 × 40 × 40 mm cube samples per mortar type were exposed to 15 cycles of salt crystallization test using a 14 % $Na_2SO_4 \times 10H_2O$ solution and following the

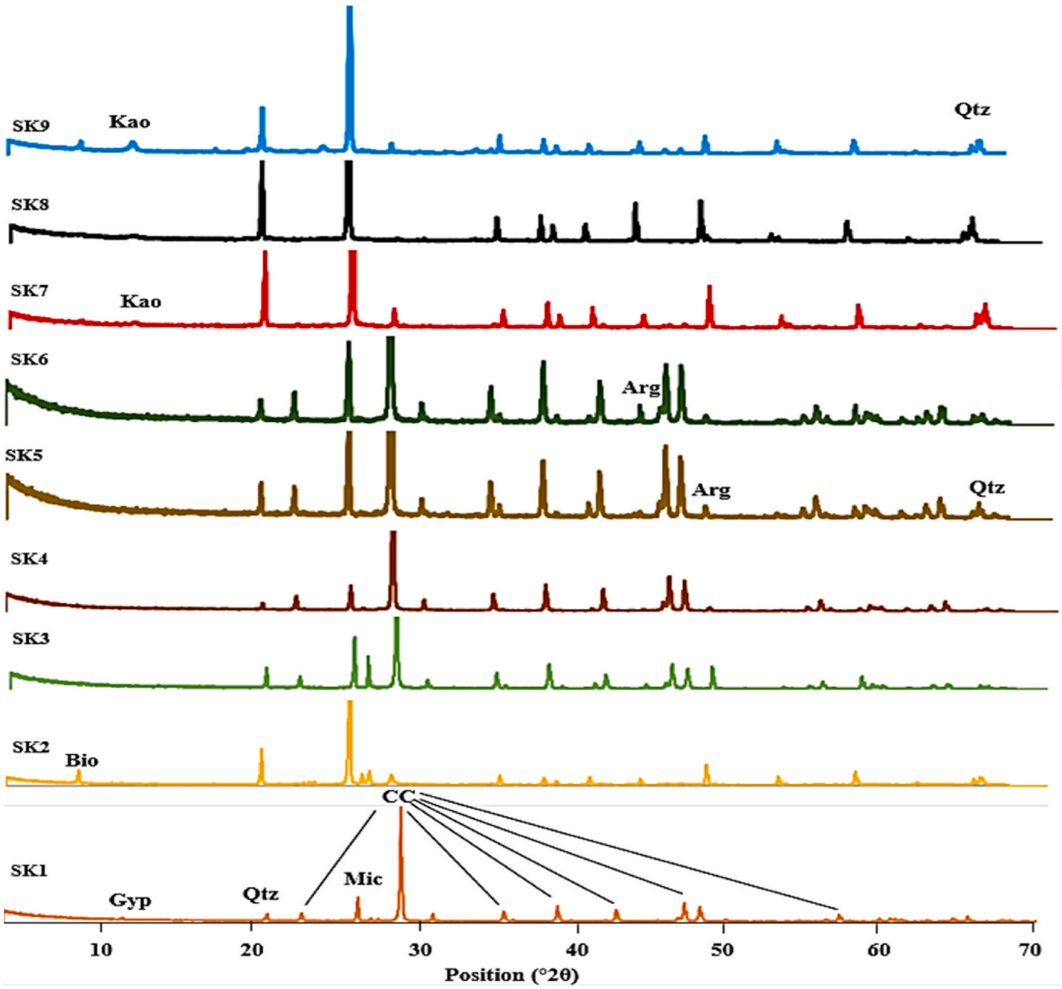

Fig. 6. Powder X-ray diffraction (PXRD) patterns of the original mortars from the Castle of Good Hope. Legend: CC - Calcite, Bio - Biotite, Qtz - Quartz, Mic - Microcline, Gyp - Gypsum, Arg - Aragonite, Kao – Kaolinite.

UNE-EN 12370 (2020) standard. Fragments loss, formation of cracks and weight variation were monitored throughout the experiment and recorded.

5. Results and discussion

5.1. Chemical composition

XRF analysis shows that samples SK1, SK3 and SK5 have the highest percentages of CaO (Table 2), suggesting that these mortars could be lime-based, confirming the visual assessment in Table 1. Based on cementation index values outlined by Ref. [40], SK1 and SK3 were prepared with a sub-hydraulic lime ($0.15 \leq CI \leq 0.3$) and very little clay content, while SK5 was prepared with a slightly hydraulic lime ($0.3 \leq CI \leq 0.5$) and an active clay of around 8 %. The other three samples, SK7, SK8 and SK9, are classified as earth mortars and are richer in silica and alumina, leading to CI outside the range (beyond the maximum CI of 1.7 provided by Ref. [40]. These results prove the absence of any of the hydraulic lime for producing these mortars with the possible addition of cement (presence of CaO in lower quantities and higher alumina content), thus verifying that these were earth mortars with active clay content above 45 %. Moreover, the higher drying/hardening rate of earth mortars, as demonstrated by high hydraulicity indices (HI) in SK7 and in SK8 and SK9, suggests the possible presence of a cement-based binder in these samples.

It is interesting to note the high CI value determined in SK2 even though this sample was visually classified as lime-based mortar. Considering the other chemical compounds, SK8 is the richest sample in Zr, which could suggest the use of dune sand deposits on the west coast (north of Cape Town) where zircon crystals are present [41,42]. MnO and P_2O_5 appear in minimal amounts (below 0.05 and 0.2 %, respectively) in all the samples. As shown in Table 4, the higher LOI content clearly corresponds to the samples with a higher amount of CaO due to the release of CO_2 during the calcination of the samples.

5.2. Mineralogical composition

The PXRD patterns show an overall composition with high amounts of calcite ($CaCO_3$), the typical mineral phase of lime mortars, except for the three earth mortars (SK7, SK8 and SK9) and SK2, which are rich in quartz (SiO_2) (Fig. 6 and Table 3). SK2 is rich in quartz but extremely poor in calcite and this composition does not match that of lime mortar. It is possible that in this case, white cement was used in the elaboration of mortar and, therefore, depending on the first use of cement in the construction industry, the mortar in question was not an original mortar but an intervention of which there is no evidence of the application date. Due to the high reflectance power of quartz and very low of phases of cement, it is very difficult to identify these last by PXRD. The earth mortars are rich in quartz with scarce kaolinite. SK5 and SK6 display considerable amounts of aragonite, the presence of which is clearly related to the mineralogy of shells used in the mortar aggregate. Some traces of gypsum are detected in SK1, SK2 and SK3, and it was probably added to help with the fast drying of the mortars. Small peaks of hematite and microcline ($KAlSi_3O_8$) are other phases identified in the samples. Biotite is also found in two of the three earth mortars (SK7 and SK8). According to the geology of Cape Town [43], it is no surprise that the original mortar samples are rich in mineral phases associated with outcropping rocks in the three main rock formations in the area, the late-Precambrian Malmesbury group (sedimentary and metamorphic rock), the Cape granite comprising the huge Peninsula, Kuilsriver-Helderberg, and Stellenbosch batholiths [7].

Fig. 7 shows four TG curves that summarize the behavior of the 8 original mortars. In detail, the blue curve indicated as Batch 1 corresponds to samples SK1, SK3, SK4, SK5 and SK6 whose trends are remarkably similar. Batch 2 (in orange) shows sample SK2; Batch 3 consists of SK7 and SK9 samples and shows similar trends to the representative SK7 shown with the grey curve; Batch 4 (in yellow) shows one sample, SK8 again. Batch 1 is characterized by only one main inflexion that starts around 700 °C and ends at 880 °C due to calcite decomposition [44], the main phase detected by PXRD in these samples (see Table 3 and Fig. 6). Batch 2 differs significantly from the previous one even though it was visually classified as lime mortar and has a somewhat similar thermogram as the earth mortars grouped in Batch 3. Batch 2 shows a first weight loss between 100 and 200 °C due to the dehydration of gypsum detected by PXRD. Then, the other two steps can be identified between 300 and 500 °C and between 500 and 700 °C due to the dehydroxylation of biotite and perhaps some portlandite, the presence of which suggests incomplete carbonation of the mortar [45]. The main loss in Batch 2, between 700 and 800 °C, is linked to calcite decomposition. Regarding Batch 3, there is no inflexion at 100–200 °C as no gypsum was added to earth mortars but a slow, steady descent up to 700 °C due to phyllosilicate dehydroxylation. Again, between 700 and 800 °C, the main loss is due to the presence of calcite in these mortars. Finally, Batch 4 is characterized by a small descent and is the

Table 3
Qualitative mineralogical composition by PXRD of the original mortars showing: very abundant ***; abundant **; scarce*; mineral in traces tr; absence of a mineral -. Legend: CC - Calcite, Bio - Biotite, Qtz - Quartz, Mic - Microcline, Gyp - Gypsum, Arg - Aragonite, Kao – Kaolinite.

Sample ID	Qtz	CC	Bio	Mic	Gyp	Arg	Kao
SK1	*	***	–	*	*	tr	–
SK2	***	*	**	tr	tr	tr	–
SK3	*	***	–	*	tr	tr	–
SK4	**	***	–	tr	tr	tr	–
SK5	**	***	–	tr	tr	*	–
SK6	**	***	–	–	tr	**	–
SK7	***	tr	tr	–	–	–	*
SK8	***	tr	tr	–	–	–	tr
SK9	***	tr	tr	–	–	–	*

Table 4
Hydric behavior of control mixes (M1 and M3) and the proposed repair mortars (M4, M6, M7 and M9). Legend: A_b - free water absorption (%); A_f - forced water absorption (%); A_x - degree of pore interconnection (%); D_i -drying index; S - saturation coefficient (%); P_o - open porosity (%); ρa - apparent density (g/cm^3); ρr - real density (g/cm^3). Standard deviations are shown in brackets.

Hydric property	M1	M3	M4	M6	M7	M9
A_b	12.86 (0.092)	12.41 (0.376)	11.20 (0.251)	9.72 (0.369)	13.82 (0.319)	15.79 (0.147)
A_f	15.45 (0.100)	15.58 (0.412)	13.06 (1.007)	11.64 (0.336)	15.69 (0.325)	16.63 (0.210)
A_x	16.77 (0.218)	20.37 (0.487)	13.95 (5.398)	16.52 (0.833)	11.90 (0.211)	5.06 (0.402)
S	70.33 (0.072)	66.04 (0.854)	73.67 (5.632)	68.63 (1.200)	78.11 (0.047)	87.69 (0.441)
D_i	0.932 (0.001)	0.930 (0.001)	0.934 (0.001)	0.939 (0.001)	0.930 (0.0003)	0.931 (0.001)
P_o	28.30 (0.146)	28.39 (0.694)	24.97 (1.551)	22.55 (0.622)	28.43 (0.607)	29.69 (0.266)
ρa	1.83 (0.003)	1.82 (0.004)	1.91 (0.028)	1.94 (0.004)	1.81 (0.005)	1.79 (0.009)
ρr	2.55 (0.003)	2.54 (0.020)	2.55 (0.015)	2.50 (0.017)	2.53 (0.024)	2.54 (0.010)

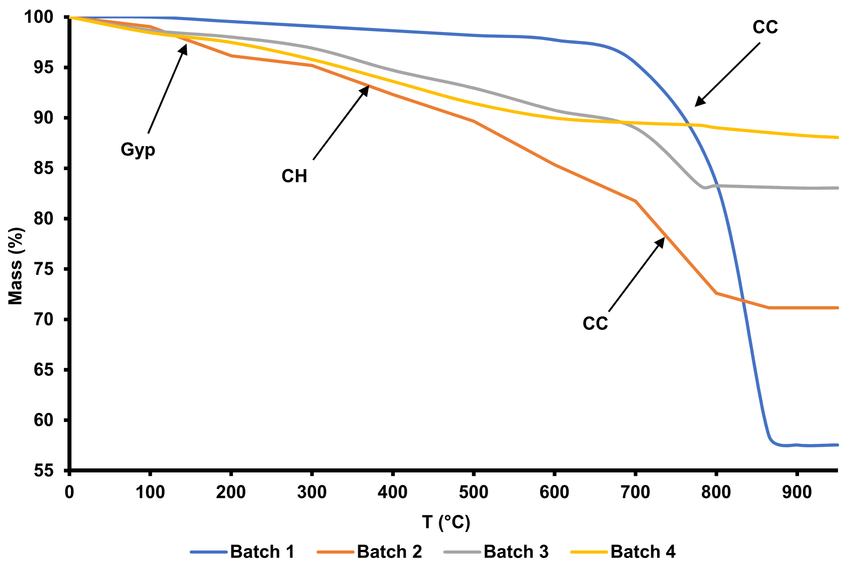

Fig. 7. TG curves for original mortars show the weight loss over increasing heating temperature over a period of time. Batch 1 mortars represented by SK1 showed similar pattern while Batch 2 represents sample SK2, Batch 3 represented by SK7 with similar pattern and Batch 4 representing SK8. Legend: Calcite-CC, gypsum-Gyp, portlandite –CH.

mortar with the lowest weight loss (about 12 %), according to the mineralogy detected by PXRD, due to the dehydroxylation of phyllosilicates that were present in traces (see Table 3).

5.3. Texture

The ESEM observations of SK1 revealed the presence of clustered flower-like morphologies [46] with aggregated particles of approximately 5 μm in size in a porous matrix (Fig. 8a). The EDS spectrum analysis of these crystals and their scalenohedral morphology suggests they are calcite. Calcite is also observed with different morphology (i.e., tabular) and denser particle distribution (Fig. 8b). Quartz grains scattered throughout the matrix have also been identified (Fig. 8b). The presence of K, Al and Si elements in SK5 suggests the presence of feldspar crystals (Fig. 8c), possibly microclines, according to PXRD analysis. The presence of Ca in the same EDS spectrum is related to the lime binder, while Na and Cl are due to the sea spray and the precipitation of halite on the surface of any coastal buildings. A cubic crystal of halite is clearly visible in the left margin of Fig. 8b. Feldspars are usually prismatic and have marked cleavage (see black arrow, Fig. 8d). Sporadic spherical contaminant particles have also been detected (Fig. 8e). They are about 2 μm in size and are rich in Si (see EDS analysis). Sometimes, organic fibers (perhaps fungal hyphae or other types of roots) can be seen in the matrix of the original mortars (Fig. 8f).

5.4. Physical properties

As shown in Table 1, the visual inspection of the nine original mortar samples collected from the Castle of Good Hope distinguished SK1 to SK6 (lime mortars) from SK7 to SK 9 (earth mortars). This observation was supported by a series of experiments described in this section. Mercury intrusion porosimetry (MIP) analysis carried out on two samples showed that plaster mortar (SK1) is more porous than the bedding (SK5) mortar (Fig. 9), with 38 % and 21 % open porosity (P_{oMIP}), respectively. SK1 shows an almost unimodal pore size distribution curve with the main peak at around 2 μm pore radius. A very small second family pores can be seen on the left of the main peak between 0.02 and 0.15 μm. SK5 presents a much less pronounced and polymodal curve with a peak at 24 μm pore radius and

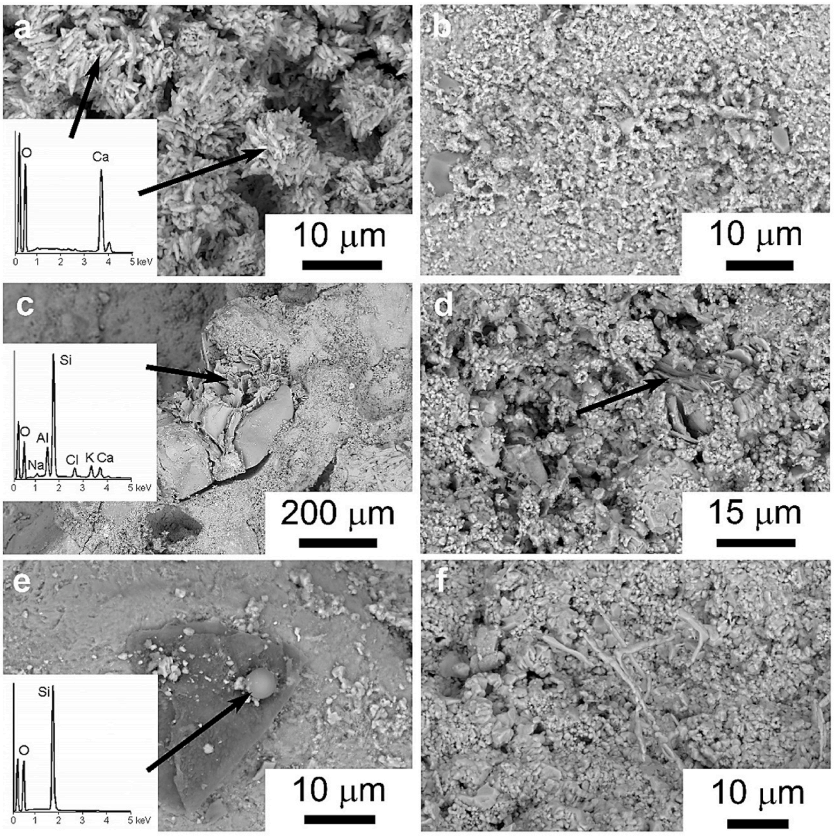

Fig. 8. ESEM micrographs and EDS spectra for samples SK1 (a–b) and SK 5 (c–f).

another sector of pores between 0.007 and 2 μm. The higher amount of smaller pores in SK5 compared to SK1 determines a slightly higher specific surface area (SSA) in the former.

5.5. Hydric behavior

For heritage repair mortars, a general expectation is to select a new mortar that will allow adequate moisture absorption and evaporation and with a similar or higher moisture evaporation rate than the substrate [21]. However, careful consideration should be taken since fast evaporation in the presence of soluble salts might lead to the development of subefflorescences and damage the surrounding materials, while slow evaporation can lead to frost action-related problems. Hydric parameters listed in Table 4 and Fig. 10 display a somewhat similar free water absorption trend (A_b, Table 4), with M9 having the highest A_b followed by M7. These two mortars (M7 and M9) portrayed the highest saturation coefficient (S) and higher porosity (P_o) than the other mortars. The control samples M1 and M3 also had higher porosity.

Sample M3 displayed the lowest pore interconnection denoted by the highest A_x value, while M9 demonstrated the highest interconnection between pores (lowest A_x in Table 4 and lowest curve slope in sector b in Fig. 10). The explanation for this difference in A_x lies in the use of the higher amount of binder in M9 (it is the only sample with a 1:1 binder-to-aggregate ratio), which may have

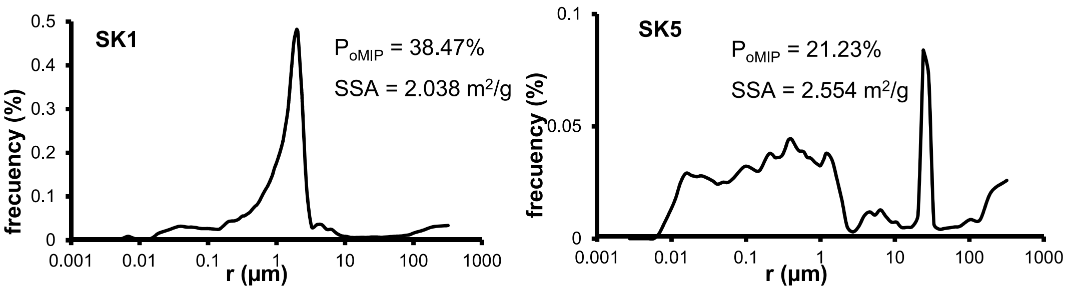

Fig. 9. Pore size distribution curves of mortars from the Castle of Good Hope obtained by mercury intrusion porosimetry. Frequency (in %) versus pore radius (in μm). Open porosity (P_{oMIP}) and specific surface area (SSA) values are indicated in each diagram.

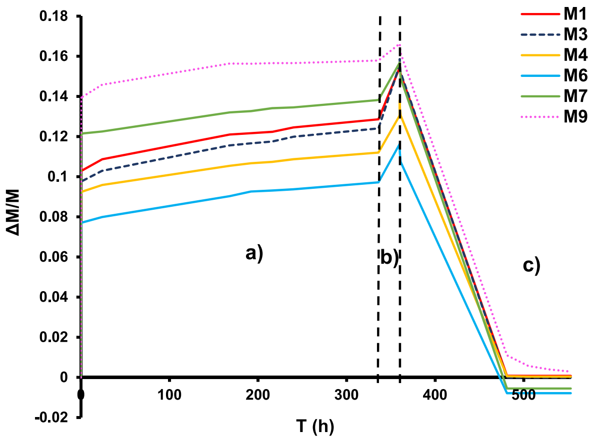

Fig. 10. Hydric behavior of new repair mortars a) Water absorption at atmospheric pressure, b) water absorption under vacuum and c) samples' drying curves. The graph shows a variation in weight (ΔM/M) versus time (in hours).

favored the development of a considerable number of retraction fissures, thus improving the circulation of water in the pore network. Note that A_x is inversely related to the saturation coefficient (S) (Table 4). This is logical since samples with poor interconnection among pores (high A_x values) saturate poorly (low S values). The lowest free (A_b) and forced (A_f) water absorptions in M6 suggest that this mortar has low retraction fissures, absorbing the least amount of water and attaining the lowest P_o and S values.

Regarding the drying of samples, control samples M1 and M3 have a similar drying pattern, as seen in segment (c) of Fig. 10. M6 was the quickest to dry (highest D_i) unlike M9, which took longer to dry. The values of real density (ρr, Table 5) are quite similar as they depend on the mineralogy of mortars. On the other hand, apparent density (ρa) is linked to the entire volume of samples (i.e., also the empty spaces). Therefore, more porous samples generally have lower ρa values or higher differences between ρa and ρr. In light of hydric tests, M6 emerged to be a preferred repair mortar option since it displayed lower water absorption properties with porosity (23 %) matching that of the original sample SK5; hence, it is less prone to water attack, resulting in higher durability expectations [47] which are to be evaluated later by salt crystallization and freeze–thaw tests. M4 could be a second option should M6 fail to meet the durability requirements. In terms of water flow in the pore system, M7 and M9 could be selected for the replacement of SK1 mortars based on their high porosity values.

5.6. Aesthetic properties

In terms of color, the new repair mortars show an almost similar lightness except for M6 and M9, which are lighter (higher L*), but less saturated (lower C*). This is because sample M6 has the lowest chromatic parameter a*, while M9 has the lowest b* (Table 5). The hue angle of samples M4 and M6 stand out from the others (h°, Table 5). Even if all samples fall in the grey area of the Munsell Soil Color Chart, all original samples, except SK4, show higher b* values. This is why when the original samples are compared with those new ones, ΔE is always greater than 5, the limit above which people can easily distinguish two colors as different [24]. M7 and M9 are the two repair mortars with the highest ΔE values compared to the original ones SK2 and SK6. However, these differences were, at least in part, expected considering that the original mortars have survived weathering conditions for over 350 years, hence, color change.

Table 5
CIELAB color space parameters: lightness (L*), chromatic parameters a* and b*, chroma (C*), and hue angle (h°) for the proposed repair mortars for the Castle of Good Hope. ΔE is the color difference between original mortars and new repair ones.

Sample ID	Sample Detail	L*	a*	b*	C*	h°	ΔE
SK1	Original sample	81.21	3.63	13.45	13.93	74.91	–
SK2	Original sample	69.93	3.33	11.11	11.59	73.36	–
SK3	Original sample	78.23	2.75	11.02	11.36	75.99	–
SK4	Original sample	74.85	1.62	5.63	5.86	73.93	–
SK5	Original sample	76.87	3.49	10.81	11.36	72.11	–
SK6	Original sample	78.57	2.66	11.64	11.94	77.17	–
M1	Repair control sample 1	83.84	1.53	6.74	6.91	77.10	–
M3	Repair control sample 2	83.92	1.63	7.03	7.22	76.95	–
M4	SK4 replacement	83.63	1.21	6.76	6.86	79.73	8.86
M6	SK5 replacement	85.06	1.13	6.24	6.35	79.65	9.66
M7	SK1 replacement	84.19	1.34	5.62	5.77	76.52	8.69
M7	SK2 replacement	84.19	1.34	5.62	5.77	76.52	15.41
M7	SK3 replacement	84.19	1.34	5.62	5.77	76.52	8.17
M9	SK6 replacement	86.22	1.41	5.28	5.47	75.02	10.03

5.7. Compactness and compressive strength

The mortars made with commercial sand (M1 and M3) are more compact than those made with sea sand (Table 6). It is also interesting to note that the lowest ultrasound velocity was measured in a mortar containing gypsum (M7). This observation disputes the assumption that gypsum was only added to aid quick setting. The addition of gypsum influences the waves' velocity in the mortar (V_p, Table 6). If this was not the case, M4 and M7 V_p were expected to be within the same range since the two mortars have the same components except for the presence of gypsum in M7. The control samples without the addition of seashell fragments are less anisotropic (ΔM) compared to the shell reinforced mortars. These organic fragments should play an important role in increasing the mortar compactness. To this respect [29],observed that the proteins present in the shells help bind the raw materials by augmenting the internal cohesion between crystalline particles, hence, higher strength and interlocked connection between particles, causing tough mortar properties.

However, the seashell fragments (and their proteins) had no impact on either the velocity as shown in Table 6 or strength as shown in Fig. 11, whilst the curing period plays the key role in the strength development of these mortars. The control (M1 and M3) and gypsum-containing mortars (M7) in their early stage of curing/carbonation (after 28 days) achieved significantly high (generally 50 % more) compressive strengths when compared to more carbonated samples (after 60 and 90 days). On the other hand, the other samples (M4 and M6) seemed to gain compressive strength over a prolonged hydration period of 90 days. Sample M9 did not follow any trends between the two described groups, showing high mortar strength at 60 curing days. This out-of-trend strength development could be due to a different mixing ratio, considering that M9 is the only mortar with a 1:1 composition. Logically, the particle sizes are smaller in this last mix (M9), with higher calcite formation through the carbonation process, contributing to increased strength. To this respect [29], suggested that the grain size between 0 and 4 mm provides the highest compressive strength, while the bigger grains reduce the mortar strength. A decrease in the compressive strength of M7 could be influenced by adding gypsum in this mortar.

5.8. Durability

The deterioration patterns for the six new mortars proposed for restoring the Castle of Good Hope due to the alternation of freezing and thawing can be seen in Fig. 12. During the test, some samples suffered a small weight increase in the first and second cycles due to the water filling the samples' pores, while other samples, such as M7, had already started to lose weight from the second cycle. Visually, the deterioration pattern of mortars is such that the edges crumble first, with weight loss happening towards the center of the sample. M6, M7 and M9 could not end the decay test, with M9 being the worst, not managing to pass the 9th cycle. According to the hydric tests, M9 was the most porous material (Po, Table 4), influencing its resistance to freeze-thaw cycles [48]. However, its open porosity is not so different from the other samples. The degree of pore interconnection is what differentiates it from the other samples (A_x, Table 4). This sample has a much lower A_x value (better pore interconnection) than the others. This will have favored an easier water migration into the capillaries of this mortar, causing its early breakage during the water-ice phase transition. The gypsum-infused mortar (M7) was the second least resistant to freeze-thaw test, as the samples broke at the 12th cycle, while M6 lasted until the 19th cycle. The other types of mortar endured 30 cycles with an average 50 % mass reduction at the end of the test.

The resistance of mortars to fifteen salt crystallization cycles was almost similar for all the samples, irrespective of their composition, except for M7, which was the mortar that lost more weight (Fig. 13). From the beginning to the 3rd - 4th cycle, all the samples gain small weight due to the crystallization of sodium sulphate in their pore system. Later on, at the 7th cycle, M7 experienced a weight loss of around 70 % instead of roughly 30 % as in the other mortars (Fig. 13). Right after this cycle, the samples started to break off, displaying signs of crumbling, with the cubes changing shape as they shed off layers from the surface to the inside. At the end of the test, there was a general 50 % mass loss for all the mortars besides M7, which lost 95 % of its mass. Benavente et al. [49] suggested that the materials' ability to withstand salt attack is related to its compressive strength and P-wave velocity. The fact that M7 is the mortar with the lowest compressive strength and ultrasound velocity can explain its poor resistance to degradation due to the crystallization of salts. Control samples (M1 and M3) performed best.

6. Conclusions

Using incompatible materials to restore historic structures is a widespread issue, with negative consequences that threaten their authenticity and often fail to resolve the problems of deterioration that plague them. The use of inappropriate materials perpetuates the need for recurrent repairs. In order to solve this problem, it is imperative to study the design and development of new mortars for heritage restoration, with compositions and performance that perfectly match the original materials.

The primary objective of this study was to investigate mortar design procedures for heritage restoration and to develop appropriate materials in compliance with existing standards, including RILEM, European and South African National Standards where applicable. By characterizing the original sub-hydraulic lime and earth-based mortars, valuable insights were gained into the production process of the new materials. The results highlighted the importance of a methodical framework for restoration professionals, particularly in developing countries where resources for restoration studies of heritage buildings are scarce.

The new repair mortar M4 had a chemical and mineralogical composition congruent with the original lime plasters (SK1 to SK3), floor mortar (SK4) and bedding mortars (SK5 to SK6), showing good resistance to ageing tests. The other mortars, M6, M7 and M9, crumbled rapidly during these tests, with M9 on the other hand showing the highest compressive strength of 1.5 MPa at 60 days. The high porosity (28.43 % and 29.69 %), free and forced water absorption rates of 13.82 % and 15.79 % in M7 and 15.69 % and 16.63 % in M9 mortar were responsible for these mortars crumbling just after the 3rd out of 15 salt crystallization cycles and after the 6th out of 30 freeze-thaw cycles. The 1:1 binder-to-aggregate ratio in sample M9 explains this mortar's higher compressive strength as opposed to other new mortars having a 1:3 ratio. Therefore, M9 has smaller particles and high calcite (from high lime content) formation which

Table 6
Ultrasound values of new repair mortars. V_{Pa}, V_{Pb} and V_{Pc} represent ultrasonic wave velocities in m/s along the three orthogonal mortar cube directions. ΔM stands for total anisotropy (%).

Mortar ID	Wave velocity (m/s)				ΔM (%)
	V_{Pa}	V_{Pb}	V_{Pc}	V_P Aver.	
M1	1841	1848	1786	1825	4.41
M3	1634	1690	1676	1667	5.31
M4	1461	1481	1544	1495	6.44
M6	1458	1580	1486	1508	8.69
M7	1189	1164	1106	1153	7.58
M9	1535	1602	1573	1570	6.00

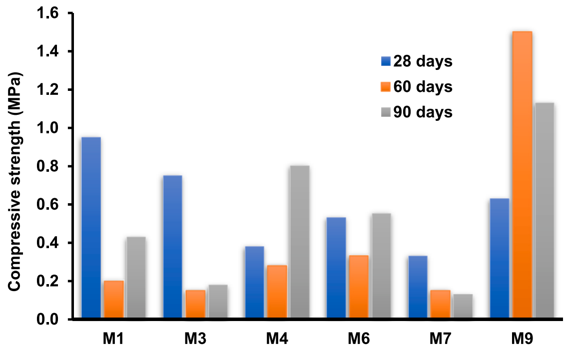

Fig. 11. Compressive strength development over curing after 28, 60 and 90 days for new repair mortars.

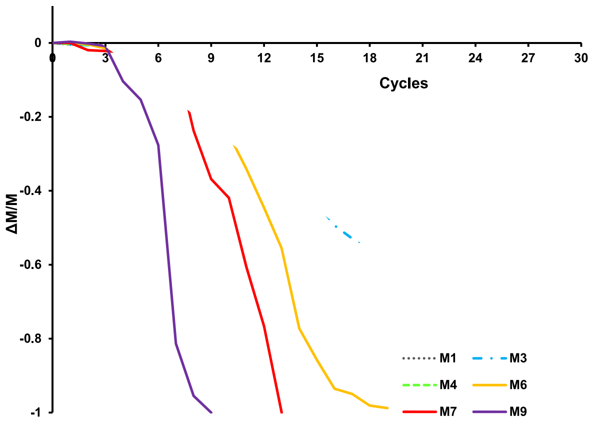

Fig. 12. Freeze-thaw test of new repair mortars. Weight variation (ΔM/M) versus number of cycles.

according to the literature, helps improve the mortar's overall compressive strength.

The aesthetic aspect, especially the colour, generally deserves attention to reduce possible inconsistencies during restoration work. The high values above 8 on color difference (ΔE) underline the need to address this aspect, possibly through color modifications using pigments, if other physical properties are not modified. In order to achieve optimal performance in masonry structures, a comprehensive study of the interaction between new mortars and substrate materials, such as stone or bricks, is essential to recommend the responsible application of these mortars.

Furthermore, the conclusion reinforces the fact that compatibility alone is not enough if skilled artisans do not carefully apply the restoration mortar. Combined with poor workmanship, a compatible mortar cannot solve the problem of premature deterioration of heritage structures. For this reason, a careful approach to the application of restoration mortars is essential and requires the expertise of skilled workers to safeguard the integrity of these valuable architectural structures. Further research into heritage-compatible application techniques for restoration mortars deserves to be explored in future research.

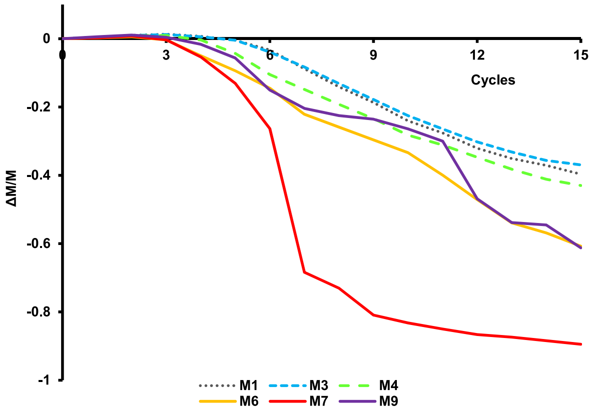

Fig. 13. Salt crystallization test of new repair mortars. Weight variation (ΔM/M) versus number of cycles.

CRediT authorship contribution statement

Maphole Emelly Loke: Writing – review & editing, Writing – original draft, Visualization, Validation, Resources, Project administration, Methodology, Investigation, Funding acquisition, Formal analysis, Data curation, Conceptualization. **Kumar Pallav:** Writing – review & editing, Supervision, Resources, Methodology, Funding acquisition. **Giuseppe Cultrone:** Writing – review & editing, Supervision, Resources, Methodology, Funding acquisition. **Chiara Di Filippo:** Methodology, Data curation.

Declaration of competing interest

The authors declare the following financial interests/personal relationships which may be considered as potential competing interests:Maphole Emelly Loke reports financial support was provided by African World Heritage Fund. Maphole Emelly Loke reports financial support was provided by Government of Lesotho. Maphole Emelly Loke reports financial support, administrative support, equipment, drugs, or supplies, and travel were provided by Cape Peninsula University of Technology - Bellville Campus. Maphole Emelly Loke reports administrative support, equipment, drugs, or supplies, and travel were provided by South African Heritage Resources Agency. Maphole Emelly Loke reports administrative support and equipment, drugs, or supplies were provided by Castle of Good hope. Maphole Emelly Loke reports equipment, drugs, or supplies was provided by Afrimat Cape Lime company. Giuseppe Cultrone reports equipment, drugs, or supplies was provided by Centro de Instrumentación Científica University of Granada. Giuseppe Cultrone reports administrative support and equipment, drugs, or supplies were provided by Research group RNM179 of the Junta de Andalucía (Spain). Giuseppe Cultrone reports administrative support and equipment, drugs, or supplies were provided by Research project B-RNM-188-UGR20 (Spain) of the Regional Ministry of University, Research and Innovation of the Junta de Andalucía and FEDER, a way of making Europe. Maphole Emelly Loke reports article publishing charges was provided by South African National Library and Information Consortium. If there are other authors, they declare that they have no known competing financial interests or personal relationships that could have appeared to influence the work reported in this paper.

Data availability

Data will be made available on request.

Acknowledgements

This study forms part of Doctoral research that is financially supported by the Government of Lesotho, the Cape Peninsula University of Technology and the African World Heritage Fund (Moses Mapesa Research Fund). The authors are grateful to the South African Heritage Resources Agency for providing sampling and export permits for transporting the test samples to Spain and the Castle of Good Hope management for their cooperation and support. We are thankful to the Centro de Instrumentación Científica of the University of Granada laboratory assistance with the XRF, ESEM and TG-DSC analyses as well as to the research group RNM179 of the Junta de Andalucía and the research project B-RNM-188-UGR20 (Spain) of the Regional Ministry of University, Research and Innovation of the Junta de Andalucía and FEDER, *a way of making Europe*. The laboratory assistance in producing the new mortars by Mr W. Snell and Mr L. Minnies at the concrete laboratory of Cape Peninsula University of Technology, South Africa, is highly appreciated.

References

[1] J. Hormes, A. Diekamp, W. Klysubun, G.L. Bovenkamp, N. Börste, The characterization of historic mortars: a comparison between powder diffraction and synchrotron radiation based X-ray absorption and X-ray fluorescence spectroscopy, Microchem. J. 125 (2016) 190–195, https://doi.org/10.1016/j.microc.2015.11.034.

[2] M.E. Loke, K. Pallav, R. Haldenwang, Characterisation of heritage cementing materials for restoration purposes: a review, J. South African Inst. Civ. Eng. 62 (2020), https://doi.org/10.17159/2309-8775/2020/V62N1A2.

[3] B. Vukindu, Investigating the Performance Requirements for Proprietary Concrete Repair Materials with Respect to Durability and Cracking Resistance, University of Cape Town, 2021. Masters Thesis.
[4] S.H. Kang, S.O. Lee, S.G. Hong, Y.H. Kwon, Historical and scientific investigations into the use of hydraulic lime in Korea and preventive conservation of historic masonry structures, Sustain. Times 11 (2019), https://doi.org/10.3390/su11195169.
[5] D.N. Kumar, P.R. Kumar, Investigations on alternate lime-pozzolana based mortars for repair of heritage structures, Construct. Build. Mater. 341 (2022) 127776, https://doi.org/10.1016/j.conbuildmat.2022.127776.
[6] M. Lukovic, Influence of interface and strain hardening cementitious composite (SHCC) properties on the performance of concrete repairs. https://doi.org/10.4233/UUID:28B07D9B-C704-47FA-9BA3-CD9FDE10130A, 2016.
[7] M.E. Loke, G. Cultrone, K. Pallav, in: T. Endo, Y. Hanazato (Eds.), A Mineralogical Study of 350-Year-Old Historical Mortars for Restoration Purposes: the Case of the Castle of Good Hope (Cape Town, South Africa), Springer Nature, 2023, pp. 271–282, https://doi.org/10.1007/978-3-031-39603-8_23.
[8] A. Feizolahbeigi, Analysis of Historical Mortars to Achieve Compatible Mortar for Restoration: Archeological Site of Dion, Greece, 2021.
[9] B. Zwarteveen, The Castle of Good Hope Research Part I Introduction and Theory, 2016.
[10] History of the Castle Of Good Hope, Castle Good Hope (n.d.). https://www.castleofgoodhope.co.za/index.php (accessed September 2, 2023).
[11] A.M.K. Ngoma, Characterisation and Consolidation of Historical Lime Mortars in Cultural Heritage Buildings and Associated Structures in East Africa, 2009.
[12] M. Abdel-Mooty, S. Khedr, T. Mahfouz, Evaluation of lime mortars for the repair of historic buildings, in: WIT Trans. Built Environ., 2009, pp. 209–220, https://doi.org/10.2495/STR090191.
[13] L. Schueremans, Ö. Cizer, E. Janssens, G. Serré, K. Van Balen, Characterization of repair mortars for the assessment of their compatibility in restoration projects: research and practice, Construct. Build. Mater. 25 (2011) 4338–4350, https://doi.org/10.1016/j.conbuildmat.2011.01.008.
[14] M. Pérez-Alonso, K. Castro, M. Álvarez, J.M. Madariaga, Scientific analysis versus restorer's expertise for diagnosis prior to a restoration process: the case of Santa Maria Church (Hermo, Asturias, North of Spain), Anal. Chim. Acta 524 (2004) 379–389, https://doi.org/10.1016/J.ACA.2004.06.034.
[15] B. Klimek, M. Grzegorczyk-Frańczak, Properties of mortars with recycled stone aggregate for the reconstruction of sandstone in historic buildings, Sustain. Times 13 (2021) 1–15, https://doi.org/10.3390/su13031386.
[16] M. Monaco, M. Aurilio, A. Tafuro, M. Guadagnuolo, Sustainable mortars for application in the cultural heritage field, Materials 14 (2021) 1–17, https://doi.org/10.3390/ma14030598.
[17] Efnarc, Specification and guidelines for self-compacting concrete. www.efnarc.org, 2002.
[18] M. Caroselli, S.A. Ruffolo, F. Piqué, Mortars and plasters—how to manage mortars and plasters conservation, Archaeol. Anthropol. Sci. 13 (2021), https://doi.org/10.1007/s12520-021-01409-x.
[19] A. Arizzi, Design of Ready-To-Use Rendering Mortars for Use in Restoration Work, University of Granada, Spain, 2012. PhD Thesis.
[20] O.S. Subbotin, Architectural and planning principles of organization and reconstruction of coastal areas, Mater. Sci. Forum 931 (MSF) (2018) 750–753, https://doi.org/10.4028/WWW.SCIENTIFIC.NET/MSF.931.750.
[21] S.K. Van Domelen, The choice is yours: considerations & methods for the evaluation & selection of susbitute materials for historic preservation. http://repository.upenn.edu/hp_theses, 2009. http://repository.upenn.edu/hp_theses/119.
[22] G. Ponce-Antón, A. Arizzi, G. Cultrone, M.C. Zuluaga, L.A. Ortega, J.A. Mauleon, Investigating the manufacturing technology and durability of lime mortars from Amaiur Castle (Navarre, Spain): a chemical–mineralogical and physical study, Construct. Build. Mater. 299 (2021), https://doi.org/10.1016/j.conbuildmat.2021.123975.
[23] EN 16085, Norma Española, 2012. www.aenor.es.
[24] W.S. Mokrzycki, M. Tatol, Colour difference δE - a survey, Mach. Graph, Vista 20 (2011).
[25] S. He, C. Jiao, Y. Niu, S. Li, Utilizing of coral/sea sand as aggregates in environment-friendly marine mortar: physical properties, carbonation resistance and microstructure, Case Stud. Constr. Mater. 16 (2022) e00981, https://doi.org/10.1016/j.cscm.2022.e00981.
[26] P. Pineda, S. Medina-Carrasco, A. Iranzo, L. Borau, I. García-Jiménez, Pore structure and interdisciplinary analyses in Roman mortars: building techniques and durability factors identification, Construct. Build. Mater. 317 (2022), https://doi.org/10.1016/j.conbuildmat.2021.125821.
[27] F. Sun, S. Wu, Q. Jiang, B. Wang, H. Zhu, Effect of multi-substance film on the surface of sea sand on mechanical properties and durability of mortar, Res. Eng. 6 (2020) 100117, https://doi.org/10.1016/j.rineng.2020.100117.
[28] R.C. Mack, Repointing mortar joints in historic masonry buildings, US Departm, 1998 books.google.co.za/books?hl=en&lr=&id=_Xa7PnZ6n7AC&oi=fnd&pg=PA3&dq=use+of+sea+sand+in+heritage+mortars&ots=CnvVhgzN7O&sig=uTtVb2TZLnYPzY7C1Q7kDlsV4hA&redir_esc=y#v=onepage&q=use of sea sand in heritage mortars&f=false 1 20 (Accessed 20 January 2024).
[29] M. Shivakumar, A. Singh, T. Selvaraj, S. Thangaraj, Production of the traditional organic mortars of padmanabhapuram palace—a characterization study on the simulated mortars for their compatibility, Buildings 12 (2022), https://doi.org/10.3390/buildings12091466.
[30] SANS 3001-AG1, Experimental Study and Classification of Natural Zeolite Pozzolan for Cement in South Africa, 2014.
[31] A. Arizzi, H. Viles, G. Cultrone, Experimental testing of the durability of lime-based mortars used for rendering historic buildings, Construct. Build. Mater. 28 (2012) 807–818, https://doi.org/10.1016/j.conbuildmat.2011.10.059.
[32] O. Cazalla, C. Rodriguez-Navarro, E. Sebastian, G. Cultrone, M.J. De la Torre, Aging of lime putty: effects on traditional lime mortar carbonation, J. Am. Ceram. Soc. 83 (2000) 1070–1076, https://doi.org/10.1111/j.1151-2916.2000.tb01332.x.
[33] K. Beck, M. Al-Mukhtar, O. Rozenbaum, M. Rautureau, Characterization, water transfer properties and deterioration in tuffeau: building material in the Loire valley—France, Build. Environ. 38 (2003) 1151–1162, https://doi.org/10.1016/S0360-1323(03)00074-X.
[34] F. Gherardi, N. Maravelaki, Conserving Stone Heritage, 2022. https://link.springer.com/bookseries/13104.
[35] Repair Mortars for Historic Masonry, n.d. http://www.rilem.net.
[36] M. Apostolopoulou, E.T. Delegou, E. Alexakis, M. Kalofonou, K.C. Lampropoulos, E. Aggelakopoulou, A. Bakolas, A. Moropoulou, Study of the historical mortars of the Holy Aedicule as a basis for the design, application and assessment of repair mortars: a multispectral approach applied on the Holy Aedicule, Construct. Build. Mater. 181 (2018) 618–637, https://doi.org/10.1016/j.conbuildmat.2018.06.016.
[37] L. Fusade, H.A. Viles, A comparison of standard and realistic curing conditions of natural hydraulic lime repointing mortar for damp masonry: impact on laboratory evaluation, J. Cult. Herit. 37 (2019) 82–93, https://doi.org/10.1016/j.culher.2018.11.011.
[38] G. Cultrone, The use of Mount Etna volcanic ash in the production of bricks with good physical-mechanical performance: converting a problematic waste product into a resource for the construction industry, Ceram. Int. 48 (2022) 5724–5736, https://doi.org/10.1016/j.ceramint.2021.11.119.
[39] M.T. Cristofaro, A. D'Ambrisi, M. De Stefano, M. Tanganelli, Mechanical properties of mortars for structural restoration of historic masonry buildings, in: Lect. Notes Networks Syst., Springer Science and Business Media Deutschland GmbH, 2022, pp. 2213–2222, https://doi.org/10.1007/978-3-031-06825-6_213.
[40] D.A. Brosnan, Characterization and degradation of masonry mortar in historic brick structures, J. Struct. 2014 (2014) 1–7, https://doi.org/10.1155/2014/859879.
[41] K. Harlow, Naturally occurring radioactive materials and the regulatory challenges to the zircon industry, J. South. African Inst. Min. Metall. 117 (2017) 409–413, https://doi.org/10.17159/2411-9717/2017/v117n5a1.
[42] O. Moumakwa, An Overview of South Africa's zircon industry and the role of BEE Directorate, Miner. Econ. (2007) 1–18, https://doi.org/10.17159/2411-9717/2017/v117n5a1.
[43] J.S. Compton, The Rocks and Mountains of Cape Town, 2004, p. 112.
[44] A. Arizzi, G. Cultrone, Mortars and plasters-how to characterise hydraulic mortars. https://doi.org/10.1007/s12520-021-01404-2/Published, 2021.
[45] M. Földvári, Handbook of Thermogravimetric System of Minerals and its Use in Geological Practice, Geological Institute of Hungary, 2011, 978-963-671-288-4.
[46] Ç.M. Oral, B. Ercan, Influence of pH on morphology, size and polymorph of room temperature synthesized calcium carbonate particles, Powder Technol. 339 (2018) 781–788, https://doi.org/10.1016/j.powtec.2018.08.066.

[47] G. Cultrone, E. Sebastián, K. Elert, M.J. de la Torre, O. Cazalla, C. Rodriguez-Navarro, Influence of mineralogy and firing temperature on the porosity of bricks, J. Eur. Ceram. Soc. 24 (2004) 547–564, https://doi.org/10.1016/S0955-2219(03)00249-8.
[48] D. Křivánková, C.L. Nunes, Z. Slížková, D. Frankeová, K. Niedoba, High-performance repair mortars for application in severe weathering environments: frost resistance assessment, Hist. Mortars (2019) 155–168, https://doi.org/10.1007/978-3-319-91606-4_12.
[49] D. Benavente, L. Linares-Fernández, G. Cultrone, E. Sebastián, Influence of microstructure on the resistance to salt crystallisation damage in brick, Mater. Struct. Constr. 39 (2006) 105–113, https://doi.org/10.1617/s11527-005-9037-0.